Contribution from the Institut für Anorganische Chemie, Universität Hannover, 3000 Hannover 1, Germany, and Department of Chemistry, Iowa State University, Ames, Iowa 50011

Synthesis and Structure of the Novel Chain Compound Nb_6I_9S and Its Hydride

H.-Jürgen Meyer*,[1] and John D. Corbett*

Received May 7, 1990

Reactions of Nb_6I_{11} or of Nb_3I_8 plus niobium with sulfur in a sealed niobium container afford Nb_6I_9S in high yield. The latter takes up hydrogen to form $Nb_6(H)I_9S$, the hydrogen presumably bonding within the metal cluster as in other niobium iodide cluster examples. The closely related structures were both refined in $P\bar{1}$ ($Z = 2$) by single-crystal X-ray diffraction means to give, for Nb_6I_9S, $a = 10.420$ (7) Å, $b = 11.592$ (5) Å, $c = 9.975$ (5) Å, $\alpha = 104.19$ (4)°, $\beta = 112.43$ (6)°, $\gamma = 105.59$ (7)°, $R = 0.045$, and $R_w = 0.045$ for 3362 independent reflections and, for $Nb_6(H)I_9S$, $a = 10.340$ (6) Å, $b = 11.554$ (8) Å, $c = 10.181$ (7) Å, $\alpha = 104.31$ (5)°, $\beta = 113.50$ (6)°, $\gamma = 105.48$ (7)°, $R = 0.072$, and $R_w = 0.049$ for 2819 independent reflections. The nominally isostructural phases consist of one-dimensional semiinfinite chains constructed from Nb_6I_8-type clusters that are interconnected by face-capping sulfur and two-bonded iodine atoms, $^1_\infty[(Nb_6I_6)S_{2/2}I_{6/2}]$, with $\bar{d}(Nb-Nb) = 2.922$ Å. The tetragonally compressed niobium octahedra in Nb_6I_9S give a distinct zigzag character to the chains and two short intercluster Nb–Nb separations near 3.36 Å. The niobium octahedra, the sulfur positions, and the chains are distinctly more regular in the hydride. Two-probe conductivity measurements on Nb_6I_9S reveal a semiconducting behavior along the chain ([111]) direction with a room-temperature conductivity of the order of 30 Ω^{-1} cm^{-1}.

Introduction

The cluster phases Nb_6I_{11}[2-4] and $CsNb_6I_{11}$[5] and their corresponding monohydrides[4,6] represent the most reduced halides known for niobium or tantalum. The two distinctive structures both contain discrete Nb_6I_8-type clusters that are interconnected by additional iodine atoms bridging between cluster vertices (I^{a-a}) to generate a three-dimensional network, viz, $(Nb_6I^i_8)I^{a-a}_{6/2}$. The 19–21 cluster-based electrons present in these leave them well short of the closed-shell count of 24 that is well recognized for M_6Y_8-type clusters of later elements, $(Mo_6Cl_8)Cl_4$, for example.[7] Less reduced molybdenum chalcogenide (Ch) cluster analogues, Mo_6Ch_8, are metallic as a result of the tighter intercluster bonding generated by the necessity that a non-metal also be bonded at all metal vertices. Related halide chalcogenide clusters are known as well, predominantly for Mo and Re, the chalcogen atoms in these preferentially occupying inner face-capping (i) positions on the clusters. Introduction of two halogen atoms per chalcogen is required to maintain a substantially fixed cluster electron count, and the greater number of anions in these mixed Ch–X compounds opens up the intercluster bridging, and the metal-like conduction characteristic is lost.[8]

Up to now, the most reduced chalcogenide halides of the heavier group 5 metals have been the tetrahedral cluster phases $Nb_4Se_4I_4$ and GaM_4Ch_8 (M = Nb, Ta; Ch = S, Se).[9] We report here a novel compound in which one-quarter of the three-bonded inner iodine atoms in $(Nb_6I^i_8)I^{a-a}_{6/2}$ have been substituted by half as many six-bonded sulfur atoms. This yields $(Nb_6I_6)S_{2/2}I_{6/2}$ with an unusual structure in which the $S^{i-i}_{2/2}$ atoms now bond opposite faces of adjoining clusters into semiinfinite chains, these connections also being bridged by $I^{a-a}_{6/2}$ atoms. As with Nb_6I_{11}, this phase also takes up hydrogen, presumably as an interstitial in the cluster center.

Experimental Section

Syntheses. The purity of the niobium metal and our preparation of Nb_6I_{11} have been described before.[5] Nb_3I_8[10] was prepared from the elements contained in a sealed fused-silica container, the temperature being slowly increased to 600 °C over 3 days with the iodine in the cooler end of the ampule. The system was isothermally homogenized for 3 days, and the product was then transported from one end of the tube to the other. Nb_6I_9S was systematically obtained from the reaction of stoichiometric amounts of niobium and sulfur with Nb_6I_{11} or Nb_3I_8. These were sealed within a niobium container that was in turn protected from oxidation by an evacuated and sealed fused-silica jacket. Conditions of 900–1080 °C and 5–10 days were useful for yields of ≥95%. Temperatures above 1000 °C produced very fibrous crystalline needles. Nb_6I_9S was also obtained from comparable reactions in the presence of RbI or CsI, and in these instances better single crystals more suitable for X-ray studies were produced. Higher amounts of sulfur yielded shiny needles of NbS_2 and fibrous NbS_3 as well. Crystals of the new chain compounds are very brittle in nature and easily fray along their needle axis. In addition, they often exhibit multiple crystal problems.

The isostructural $Nb_6(H)I_9S$ was first prepared by allowing approximately 650 Torr of H_2 (excess) to react with Nb_6I_9S at 300 °C for 4, 12, or 24 h, respectively. The X-ray powder patterns from the series were very similar but significantly and similarly shifted. A sample prepared at 250 °C for 12 h showed barely visible lineshifts. These results suggested incomplete conversions were occurring, and so another series of reactions of Nb_6I_9S (ca. 200 mg) with excess (≤500 Torr) hydrogen were run in a sealed thick-walled silica tubing (ca. 20 cm^3). These were heated to 400–550 °C over 3 days, held there for 4 days, and cooled slowly. The products all exhibited consistent and greater lineshifts and similar lattice constants, and a single needle crystal suitable for X-ray data collection was selected from a 400 °C reaction. The lattice constant data in Table I illustrate the similarity of the two phases and the plateau resulting from progressive hydrogenation. The conversion of Nb_6I_9S to $Nb_6(H)I_9S$ at 400 °C results in clear decreases in a and b, while c and β increase.

Synthetic products were characterized by X-ray powder patterns (monochromated Cu Kα radiation) obtained with the aid of an Enraf-Nonius (FR-552) Guinier camera and α-quartz as an internal standard. Lattice parameters for the title compounds were calculated by least-squares procedures from powder pattern data indexed on the basis of the single-crystal structure solutions.

Other Reactions. We had no success in producing the selenide or bromide analogue of Nb_6I_9S or its hydride. No such product was evident with a Ta_6I_9S stoichiometry either, the reaction giving Ta_6I_{14}[11] in high yield instead. Some exploratory reactions looking for a chloride analogue of Nb_6I_9S were carried out in tantalum containers. The loaded composition Nb_6Cl_9S yielded no fibrous product, and only crystals of Nb_6Cl_{14}[12] were identified via Guinier and precession examinations. A semiquantitative analysis with the aid of an electron microscope gave the composition $Nb_{5.2}Ta_{0.9}Cl_{13.9}$. No further work was done on this subject since there was no change in the space group *Bbcm* known for Nb_6Cl_{14}, and therefore niobium and tantalum had to be disordered in the structure. The Nb–Cl and Ta–Cl distances usually differ by no more than 0.03 Å.[13]

Properties. Nb_6I_9S is visually stable in air and does not show any change in the powder pattern even after several weeks. It does not react

(1) Universität Hannover.
(2) Bateman, L. R.; Blount, J. F.; Dahl, L. F. *J. Am. Chem. Soc.* **1966**, *88*, 1082.
(3) Simon, A.; von Schnering, H.-G.; Schäfer, H. *Z. Anorg. Allg. Chem.* **1967**, *355*, 295.
(4) Imoto, H.; Simon, A. *Inorg. Chem.* **1982**, *21*, 308.
(5) Imoto, H.; Corbett, J. D. *Inorg. Chem.* **1980**, *19*, 1241.
(6) Simon, A. *Z. Anorg. Allg. Chem.* **1967**, *355*, 311.
(7) Simon, A. *Angew. Chem.* **1988**, *27*, 158.
(8) Perrin, A.; Sergent, M. *J. Less-Common Met.* **1988**, *137*, 241.
(9) Yaich, H. B.; Jegaden, J. C.; Potel, M.; Sergent, M.; Rastogi, A. K.; Tournier, R. *J. Less-Common Met.* **1984**, *102*, 9.
(10) Simon, A.; von Schnering, H.-G. *J. Less-Common Met.* **1966**, *11*, 31.
(11) Bauer, D.; von Schnering, H.-G.; Schäfer, H. *J. Less-Common Met.* **1965**, *8*, 388.
(12) Simon, A.; von Schnering, H.-G.; Wöhrle, H.; Schäfer, H. *Z. Anorg. Allg. Chem.* **1965**, *339*, 155.
(13) Bauer, D.; von Schnering, H.-G. *Z. Anorg. Allg. Chem.* **1968**, *361*, 259.

0020-1669/91/1330-0963$02.50/0

Table I. Lattice Parameters and Cell Volumes for Nb_6I_9S (I) and $Nb_6(H)I_9S$ (II) from Guinier Powder Patterns[a]

	conditions, °C/days	a, Å	b, Å	c, Å	α, deg	β, deg	γ, deg	V, Å^3
I	1080/12	10.420 (7)	11.592 (5)	9.975 (5)	104.19 (4)	112.43 (6)	105.59 (7)	987 (1)
II	300/1	10.375 (8)	11.615 (5)	10.017 (6)	104.26 (4)	112.43 (4)	105.62 (4)	988 (1)
II[b]	400/4	10.340 (6)	11.554 (8)	10.181 (7)	104.31 (5)	113.50 (6)	105.48 (7)	985 (1)
II	400/3	10.336 (4)	11.549 (5)	10.178 (5)	104.22 (5)	113.49 (4)	105.42 (4)	985.5 (7)
II	550/4	10.331 (9)	11.531 (9)	10.189 (8)	104.09 (6)	113.71 (6)	105.45 (7)	984 (3)

[a] Room-temperature data, λ = 1.540 56 Å. [b] Data crystal source.

Table II. Selected Crystal and Refinement Data[a]

	Nb_6I_9S	$Nb_6(H)I_9S$
space group, Z	$P\bar{1}$, 2	$P\bar{1}$, 2
μ(Mo Kα), cm^{-1}	163.6	162.9
transm coeff, normalized	0.65–1.0	0.70–1.0
no. data with $F_o^2 > 3\sigma(F_o^2)$	3362	2819
no. params refined	145	145
R[b]	0.045	0.072
R_w[c]	0.045	0.049

[a] Lattice constant data in Table I. [b] $R = \sum||F_o| - |F_c||/\sum|F_o|$. [c] $R_w = [\sum w(|F_o| - |F_c|)^2/\sum w(F_o)^2]^{1/2}$; $w = 1/\sigma_F^2$.

with water, HCl, HNO_3, or NaOH (~0.2 M) or form the hydride therefrom, but the compound decomposes in concentrated acids after 1 or 2 days. It behaves like a lubricant when ground and becomes very shiny when pressed into a pellet. In contrast, $Nb_6(H)I_9S$ slowly decomposes in moist air with the evolution of H_2S. No NMR signals were found for ^1H or ^{93}Nb in the latter at room temperature on a Bruker solid-state unit.

Crystallography. Needle-shaped single crystals of both compounds were sealed in thin-walled glass capillaries in a glovebox. Single-crystal film work on the ternary phase showed it to be monoclinic. Detailed data collection and refinement parameters are given in the supplementary material, while a summary is given in Table II. Data were corrected for absorption empirically with ψ scans for Nb_6I_9S (in Ames) and with the crystal dimensions for $Nb_6(H)I_9S$ (in Berlin). The structure of Nb_6I_9S was solved with the direct-methods program MITHRIL[14] starting with an Nb_3 triangle located close to the inversion center in $P\bar{1}$ so as to generate a metal octahedron. The refinement employed successive cycles of full-matrix least-squares refinements and the SHELX76[15] programs. The R index converged at 4.5% (R_w = 4.5%) for Nb_6I_9S and at 7.2% (R_w = 4.9%) for the hydride. The small crystal available for the hydride, ~0.04 × 0.04 × 0.22 mm or about one-eigth of the volume of the other, and an absorption correction of limited quality are thought to be responsible for the larger R value. Hydrogen was not located but was assumed to occupy the interstitial position within the cluster, consistent with the significant increase of the size of the clusters in $Nb_6(H)I_9S$ (below) and closely analogous to the behaviors of Nb_6I_{11}[6] and $CsNb_6I_{11}$[5] on hydrogenation.

Electrical Conductivity. The temperature variation of the resistivity of a needle-shaped crystal (~0.025 × 0.025 × 1 mm) of Nb_6I_9S was measured parallel to the [111] (chain) direction (under He) with the aid of a two-probe method and a conventional cryostat. Although the crystals appear to be stable in the air for at least several weeks, they were nonetheless handled in an argon-filled glovebox prior to the conductivity experiment. Contacts were made by InGa, which provided fairly good adhesion. The resistance was measured between 40 and 300 K in the frequency region 1 kHz to 1 MHz with a Hewlett-Packard 59501B temperature programmer and 4192A LF impedance analyzer. The specific conductivity was calculated from the measured resistance (R) and the crystal dimensions as $\sigma = l/(AR)$, where l is the length and A is the cross section of the crystal between the contacts. Suitable data were obtained at 10 Hz where the imaginary contribution to the impedance was negligible. The sample resistance was measured for three different specimens in a cyclic procedure, first by cooling and then on heating. The InGa contacts on only one crystal were sufficiently good to allow the whole temperature cycle to be covered. The reproducibility of the results suggested that contact resistance, or at least its variation from sample to sample, was not a major factor.

Results and Discussion

The novel Nb_6I_9S does not appear to have any stable analogues, as might be achieved by altering the metal (Ta), the halogen (Br), or the intercluster bridging atom (Se, P, As). Hydrogen is readily taken up by Nb_6I_9S to form the presumed $Nb_6(H)I_9S$, closely analogous to reactions forming $Nb_6(H)I_{11}$[6] and $CsNb_6(H)I_{11}$.[5] Interestingly, very small amounts of $Nb_6(H)I_9S$ were first seen some years ago as a product of niobium–iodine reactions in the presence of unknown impurities.[16] The sulfur was not recognized in microprobe studies because of an accidental interference by niobium, and the crystals available were sufficiently only to determine the chain repeat length. In hindsight, the sulfur source was probably the remnants of sulfuric acid based solution that had been used to clean the niobium tubing container after the first end had been crimped and welded.

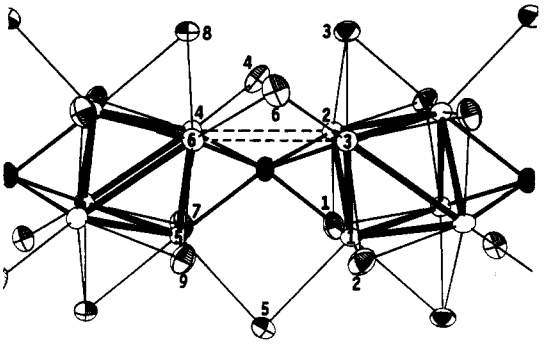

Figure 1. Two bridged cluster units in Nb_6I_9S and the atom-numbering scheme. Niobium atoms are open ellipsoids connected by heavy lines, while the sulfur atoms are solid, and the iodines, shaded. The shorter intercluster interactions are dashed. Each cluster contains a center of symmetry. (Thermal ellipsoids at 90% probability.)

The structural parameters for Nb_6I_9S and $Nb_6(H)I_9S$ are given in Table III, while important distances appear in Table IV. Anisotropic atom displacement parameters and structure factor data for the two structural studies are available as supplementary material.

Previous examples of niobium iodide clusters have all contained Nb_6I_8 units interconnected via six outer iodine atoms, viz $(Nb_6I_8)^{a-a}{}_{6/2}$, so as to generate layers of clusters. The new Nb_6I_9S and its isostructural hydride exhibit a related, yet distinctly different, connectivity. This and the atom identification are shown in Figure 1 for the former. The phases each contain two crystallographically different, centric, and approximately D_{3d} niobium octahedra (Nb1–3 and Nb4–6) that are substantially identical in their dimensions. The six triangular faces about the waist of each metal cluster that lie approximately parallel to the chain axis are capped by iodine to give Nb_6I_6 units. Each cluster is then interconnected to two others both by sulfur atoms that cap the remaining triangular faces of the Nb_6I_6 clusters and by outer iodine atoms that bridge between niobium vertices of these faces. This gives one-dimensional, semiinfinite chains that can be described as $^1_\infty[(Nb_6I^i_6)S^{i-i}{}_{2/2}I^{a-a}{}_{6/2}]$. Two orthogonal views of the chains in Nb_6I_9S are shown in Figure 2. Sulfur is seen to be located in a distorted trigonal prism of niobium atoms, the approximately parallel edges of which are bridged by iodine. Significant distortions of the individual clusters are also evident.

Adjoining chains in these structures are held together only by van der Waals interactions, accounting for the exceedingly fibrous nature of the compounds. This is emphasized if Figure 3 with a view of Nb_6I_9S along the pseudo 3-fold axis. A quick look at the structure, especially in this projection, suggests the possibility

(14) Gilmore, C. J. MITHRIL. University of Glasgow, 1983.
(15) Sheldrick, G. M. SHELX76. University of Cambridge, 1976.
(16) Smith, J. D.; Westrich, B. J.; Corbett, J. D. Unpublished research, 1981–1982.

Table III. Positional Parameters for Nb_6I_9S and $Nb_6(H)I_9S$

	Nb_6I_9S			$Nb_6(H)I_9S$[a]		
atom	*x*	*y*	*z*	*x*	*y*	*z*
Nb1	0.5136 (2)	0.0734 (2)	0.6862 (2)	0.5170 (3)	0.0846 (2)	0.7110 (3)
Nb2	0.7441 (2)	0.0407 (2)	0.6118 (2)	0.7429 (3)	0.0398 (2)	0.6133 (3)
Nb3	0.5590 (2)	0.1889 (1)	0.4773 (2)	0.5531 (3)	0.1791 (2)	0.4783 (3)
I1	0.3089 (1)	0.0593 (1)	0.1697 (1)	0.3034 (2)	0.0557 (2)	0.1681 (2)
I2	0.3409 (1)	0.2213 (1)	0.5747 (1)	0.3354 (2)	0.2197 (2)	0.5749 (2)
I3	0.7523 (1)	0.1203 (1)	0.3639 (1)	0.7590 (2)	0.1219 (2)	0.3751 (2)
I4	0.0605 (1)	0.0935 (1)	0.7588 (2)	0.0652 (2)	0.0992 (2)	0.7691 (2)
I5	0.5747 (1)	0.2266 (1)	0.0022 (1)	0.5573 (2)	0.2182 (2)	0.0112 (2)
I6	0.6409 (1)	0.4331 (1)	0.4496 (1)	0.6436 (2)	0.4285 (2)	0.4635 (2)
Nb4	0.0260 (2)	0.3227 (2)	0.8956 (2)	0.0310 (3)	0.3288 (2)	0.9043 (3)
Nb5	0.8468 (2)	0.4068 (2)	0.0204 (2)	0.8188 (3)	0.3863 (2)	0.0135 (3)
Nb6	0.8433 (2)	0.4722 (2)	0.7615 (2)	0.8517 (3)	0.4760 (2)	0.7768 (3)
I7	0.0076 (1)	0.2569 (1)	0.1497 (1)	0.0047 (2)	0.2532 (2)	0.1456 (2)
I8	0.0598 (1)	0.4233 (1)	0.6702 (1)	0.0698 (2)	0.4288 (2)	0.6842 (2)
I9	0.3396 (1)	0.4608 (1)	0.1046 (1)	0.3513 (2)	0.4692 (2)	0.1102 (2)
S	0.7545 (5)	0.2505 (4)	0.7417 (5)	0.7513 (7)	0.2490 (6)	0.7489 (7)

[a] Hydrogen atoms are at 0, $^1/_2$, 0, and $^1/_2$, 0, $^1/_2$.

Table IV. Important Bond Distances (Å) in Nb_6I_9S and $Nb_6(H)I_9S$[a]

bond	Nb_6I_9S	$Nb_6(H)I_6S$	bond	Nb_6I_9S	$Nb_6(H)I_6S$
Nb1–Nb2	2.855 (2)	2.997 (4)	Nb3–I1	2.827 (2)	2.828 (3)
Nb1–Nb3	2.850 (2)	2.958 (4)	Nb3–I2	2.861 (2)	2.893 (3)
Nb1–Nb2′	2.805 (2)	2.956 (4)	Nb3–I3	2.847 (2)	2.877 (3)
Nb1–Nb3′	2.802 (2)	2.888 (4)	Nb3–I6	2.844 (2)	2.853 (3)
Nb2–Nb3	3.068 (2)	2.998 (4)	Nb4–I7	2.875 (2)	2.894 (3)
Nb2–Nb3′	3.165 (2)	3.014 (4)	Nb4–I8	2.863 (2)	2.882 (3)
			Nb4–I9	2.817 (2)	2.815 (3)
Nb4–Nb5	2.849 (2)	2.976 (4)	Nb4–I4	2.854 (2)	2.858 (3)
Nb4–Nb6	3.064 (2)	2.984 (4)	Nb5–I7	2.916 (2)	2.906 (3)
Nb4–Nb5′	2.813 (2)	2.971 (4)	Nb5–I8	2.833 (2)	2.826 (3)
Nb4–Nb6′	3.145 (2)	2.985 (4)	Nb5–I9	2.895 (2)	2.885 (3)
Nb5–Nb6	2.852 (2)	2.954 (4)	Nb5–I5	2.943 (2)	2.872 (3)
Nb5–Nb6′	2.799 (2)	2.888 (4)	Nb6–I7	2.832 (2)	2.829 (3)
Nb3–Nb6[b]	3.374 (2)	2.509 (4)	Nb6–I8	2.868 (2)	2.896 (3)
Nb2–Nb4[b]	3.358 (2)	3.409 (4)	Nb6–I9	2.867 (2)	2.901 (3)
Nb1–Nb5[b]	3.965 (2)	3.557 (4)	Nb6–I6	2.850 (2)	2.858 (3)
Nb1–I1	2.905 (2)	2.898 (3)	Nb1–S	2.536 (5)	2.467 (7)
Nb1–I2	2.912 (2)	2.912 (3)	Nb2–S	2.408 (5)	2.430 (7)
Nb1–I3	2.830 (2)	2.820 (3)	Nb3–S	2.410 (5)	2.449 (7)
Nb1–I5[c]	2.930 (2)	2.866 (3)	Nb4–S	2.417 (5)	2.436 (7)
Nb1–I1	2.863 (2)	2.867 (3)	Nb5–S	2.544 (5)	2.464 (7)
Nb2–I2	2.825 (2)	2.821 (3)	Nb6–S	2.415 (4)	2.454 (7)
Nb2–I3	2.864 (2)	2.865 (3)			
Nb2–I4	2.860 (2)	2.854 (3)			

[a] Primed atoms are inversion related. [b] Intercluster distances. [c] The last-listed *d*(Nb–I) for each metal is the cluster-bridging (exo) distance.

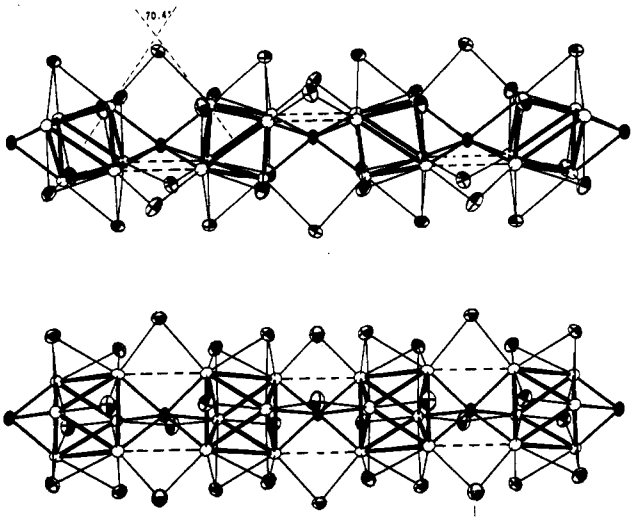

Figure 2. Two views 90° apart of a portion of the infinite chains in Nb_6I_9S that run parallel to [111] (Nb = empty, S = solid, I = shaded ellipsoids, 90% probability).

of a symmetry higher than $P\bar{1}$, since the two independent clusters are identical within the limits of error. However, significant

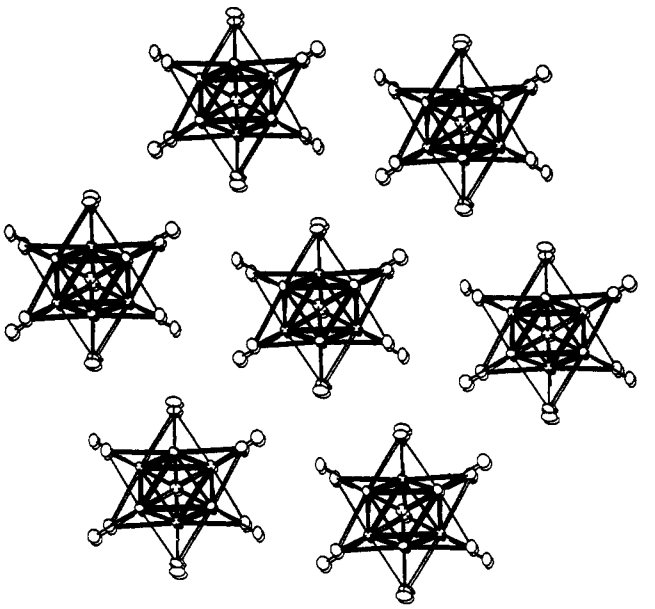

Figure 3. Projection of the structure of Nb_6I_9S slightly off [111]. Note the symmetry reduction deriving from both the nonlinear chain of sulfur atoms in the center of the chain and the outward lying 15^{a-a} atoms.

distortions (discussed below) in the bridges in Nb_6I_9S preclude 3-fold (or 6_3) symmetry. Mirror planes appear possible perpendicular to and within a single chain (Figure 2), but these are inconsistent with the rest of the structure. Rotation photographs did not reveal any mirror plane perpendicular to the [111] chain axis.

Interestingly, 19 cluster-based electrons remain in Nb_6I_9S after the non-metal valence orbitals are filled, the same as in Nb_6I_{11}, and their hydrides compare similarly. The addition of hydrogen adds one more electron to the bonding set *and* additional central bonding. The average Nb–Nb distance within the distorted clusters in Nb_6I_9S, 2.924 Å (bond order n = 0.44; total PBO/e_2 = 0.62), is somewhat longer than that in Nb_6I_{11}, 2.850 Å (n = 0.58), and $Cs_6Nb_6I_{11}$, 2.85 Å, perhaps because there are two additional intercluster Nb–Nb contacts of ~3.36 Å (n = 0.082 each) along the infinite chain. (The latter are shown dashed in Figure 2). These rather close intercluster contacts presumably correlate with the cluster distortions and with the strong Nb–S intercluster bonds. The last range from 2.408 to 2.544 Å in Nb_6I_9S and 2.430 to 2.467 Å in $Nb_6(H)I_9S$, comparable to those in NbS_3, 2.432–2.561 Å.[17] The Nb–I distances show nothing unusual relative to those in previously known cluster examples.

(17) Rijnsdorp, J.; Jellinek, F. *J. Solid State Chem.* **1978**, *25*, 325.

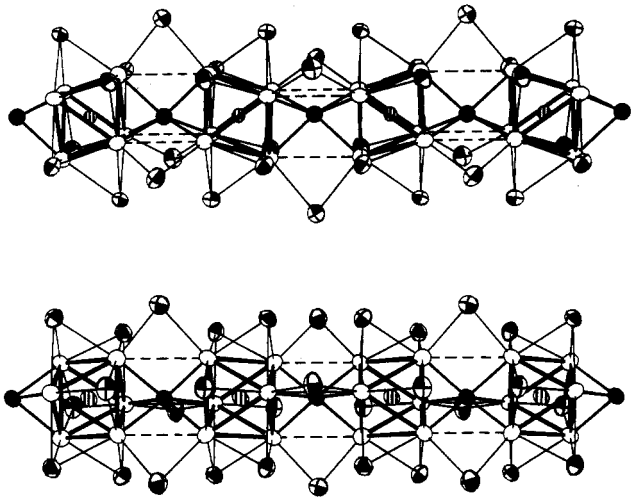

Figure 4. Two views 90° apart of the chain in $Nb_6(H)I_9S$, with atom identifications the same as in Figure 1 plus the hydrogen atom striped.

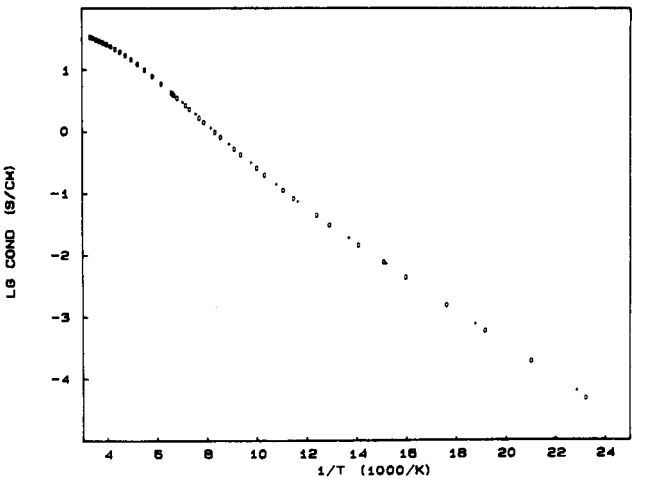

Figure 5. $\log_{10}$ conductivity (Ω^{-1} cm^{-1}) vs reciprocal temperature (K) of a single crystal of Nb_6I_9S along the chain direction: (O) heating; (+) cooling.

Cluster Distortions. Each cluster in Nb_6I_9S is significantly distorted from an octahedron via tetragonal compressions along the axes between the inversion-related Nb1–Nb1′ and Nb5–Nb5′ (Figure 1). Thus, the eight Nb–Nb distances from these atoms to the other metal atoms in the same cluster average 0.28 Å less than between the remaining four atoms (Nb2–4,6) around the waist, 3.011 Å. These waist metal atoms are also involved in the weaker intercluster metal–metal interactions, Nb2–Nb4 at 3.358 (2) Å and Nb3–Nb6, 3.374 (2) Å (Figure 1), while the third Nb1–Nb5 separation is much greater, 3.965 (2) Å. A parallel expansion of the waist within each cluster (Nb2–4,6) can also be considered a part of the cluster distortion. Sulfur is unsymmetrically bonded to the triangular faces, paralleling the above cluster distortions, so that the Nb1–S and Nb5–S distances are 0.13 Å longer than the other four. The sulfur is 0.19 Å off the center of the Nb_6 stacks, corresponding to a S–S–S angle of 175.6 (2)°.

Geometrically, the tetragonal compression of the separate clusters along Nb1–Nb1′ and Nb5–Nb5′ just described correlates very well with the obvious tilt between the pairs of cluster faces that are bridged by sulfur (Figures 1 and 2). Thus, the dihedral angle between the waist planes[18] of adjoining octahedra (3–2–3′–2′ and 4–6–4′–6′) is 70.4 (1)° (Figure 2). An increase of this by twice the 54.74° angle between the waist and a triangular face of an *ideal* octahedron would produce a substantially ideal 179.9° dihedral angle between opposed triangle faces across the bridge. In other words, the distortions seen along the chains arise from the intracluster tetragonal compression/expansion already considered, not a tilting of adjacent clusters. The cluster distortions that drive the sulfur atom off the ideal 3-fold axis and give each cluster an effective tetragonal compression are doubtlessly complex and electronic in origin. A Peierls-like distortion appears to be indicated by the results of the extended-Hückel band calculations presently underway.[19]

Hydrogen Uptake. The cluster becomes more symmetrical on forming $Nb_6(H)I_9S$ via a sizable anisotropic expansion, particularly a drastic increase along the compression axes noted above, by 0.545 (5) Å for Nb1–Nb1′ and 0.549 (5) Å for Nb5–Nb5′, along with an average 0.15-Å shrinkage in niobium separations in the waists of the two independent clusters. The two orthogonal views of the hydride shown in Figure 4 emphasize the greater regularity of the chains relative to that in Nb_6I_9S (Figure 2). Thus, the two clusters in $Nb_6(H)I_9S$ exhibit internal trans distances Nb_x–Nb'_x (x = 1–6) of 4.090 (4), 4.324 (4), 4.177 (4), 4.291 (4), 4.118 (4), and 4.144 (4) Å, respectively, with an average of 4.127 Å. A pseudomirror plane containing the distortion is no longer present. The intercluster Nb–Nb distances likewise become larger and more nearly equal on hydrogen addition ($\bar{d}$ = 3.492 Å), while the angle at the more open iodine bridge (Nb1–I5–Nb5) has decreased from 84.9 (1) to 76.6 (1)° (vs 73.3 and 75.8° at I4 and I6). On the other hand, the dihedral angle between waist planes in adjacent clusters used above to define the distortion in Nb_6I_9S (Figure 2) does not change significantly in the hydride (71.6 (1)°), and the dihedral angle between the sulfur-bridged faces of adjoining clusters is 181.1°. The sulfur atoms are now located only slightly (0.05 Å) off the centers of the Nb_3 stacks, and ∠S–S–S is 179.0 (2)°. The range of Nb–S distances is now only 27% (0.037 (10) Å) of that in the compound without hydrogen.

According to our results from different synthetic conditions, the hydrogen uptake by Nb_6I_9S appears to be a continuous process. Thus, the a and b axes shrink, while the c axis expands, β increases, and the unit cell volume decreases slightly (Table I). The volumes of the niobium octahedra actually increase on hydride formation, from 17.2 Å^3 each in Nb_6I_9S to 18.5 and 18.3 Å^3 in the hydride. Obviously, much of the necessary volume for H^- is already present in the "empty" cluster.

Conductivity of Nb_6I_9S. The extremely fibrous character of Nb_6I_9S is consistent with the presence of quasi one-dimensional infinite chains generated by intercluster bridging only along the needle axis. The compound exhibits a semiconducting (or semimetallic) characteristic along this chain ([111]) direction, as shown by the log σ vs $1/T$ results in Figure 5. A more insulating property would be expected along orthogonal directions. Values for the resistivity increase by about 6 magnitudes on cooling from room temperature to ~40 K, namely from the order of 0.03 Ω cm to 3.2 × 10^4 Ω cm, depending somewhat on errors in the cross-section measurement and any contribution from contact resistance. The plot deviates slightly from ideal Arrhenius behavior, with apparent activation energies between 0.048 and 0.070 eV, corresponding to a very narrow apparent band gap around 0.1 eV ($=2E_a$). The activation energy may be associated with surmounting the sulfide (and iodide) bridges. Cluster distortion and the resulting low symmetry in the chain presumably play an important role in conduction properties of Nb_6I_9S. Its magnetic susceptibility shows a weak paramagnetism and no evidence of a phase transition between 5 and 400 K.[19]

All metal–metal bonding states in an M_6 cluster containing 24 electrons are expected to be filled, and a high symmetry should result. Such apparently occurs in $Mo_6I_8Se_2$,[20] which shows basically the same intercluster connectivity as Nb_6I_9S but with the second selenium atom disordered among the waist I^i positions. A more symmetrical packing arrangement is indicated by the space groups $P6_3$ or $P6_3/m$. However, the very fibrous, small crystals of $Mo_6I_8Se_2$ available led to considerable difficulty in defining the structure well.[21] Even this incomplete characterization

(18) Spek, A. L. PLATON. University of Utrecht, 1982.
(19) Meyer, H.-J.; Miller, L. L.; Guloy, A.; Corbett, J. D. Research in progress.

(20) Perrin, C.; Sergent, M. *J. Chem. Res. M* **1983**, 38.

supports the notion that distortions in the niobium iodide analogues are electronic in origin. Comparison with the other niobium iodide clusters and their hydrides must await the results of bond calculational and magnetic susceptibility studies presently underway.[19]

Acknowledgment. We thank Dr. C. Rüscher (Institut für Mineralogie, Universität Hannover) for the help with the conductivity measurements, Professor J. Pickardt (Technische Universität, Berlin) for providing the diffractometer for one study, and the Deutsche Forchungsgemeinschaft for financial support of H.-J.M. This research was in part also supported by the National Science Foundation, Solid State Chemistry, via Grants DMR-8318616 and -8902954, and this portion was carried out in facilities of Ames Laboratory, DOE.

(21) The $Mo_6I_8Se_2$ refinement led to $R/R_w = 0.179/0.158$ for data to $2\theta = 50°$. The positional σ's were 0.03-0.05 Å, and the thermal parameters could not be refined.

Supplementary Material Available: Tables of crystal data and anisotropic displacement parameters for Nb_6I_9S and $Nb_6(H)I_9S$ (2 pages); tables of observed and calculated structure factor data (36 pages). Ordering information is given on any current masthead page.

Contribution from the Department of Chemistry, The University, Southampton, SO9 5NH, England

Coordination Chemistry of Higher Oxidation States. 37.[1] Tellurato Complexes of Palladium(IV) and Platinum(IV). Crystal Structures of $Na_8K_2H_4[Pd_2Te_4O_{24}H_2]\cdot 20H_2O$ and $K_6Na_2[Pt(OH)_2(HTeO_6)_2]\cdot 12H_2O$

William Levason,* Mark D. Spicer, and Michael Webster

Received July 3, 1990

The reactions between $[MCl_6]^{2-}$ (M = Pd, Pt) and telluric acid in aqueous sodium or potassium hydroxide have been shown to give Pd(IV) or Pt(IV) tellurate complexes, which have been isolated as their hydrated salts. The compounds have been studied by ^{125}Te and ^{195}Pt NMR spectroscopy, EDX, EXAFS, and single-crystal X-ray diffraction. The structure of $Na_8K_2H_4[Pd_2Te_4O_{24}H_2]\cdot 20H_2O$ has been determined. It crystallizes in the triclinic space group $P\bar{1}$, with $a = 7.403$ (1) Å, $b = 11.929$ (2) Å, $c = 12.429$ (2) Å, $\alpha = 100.28$ (1)°, $\beta = 104.92$ (1)°, $\gamma = 92.23$ (1)°, $V = 1039.4$ Å^3, and $Z = 1$. The structure was refined to $R = 0.042$ from 2146 data ($F > 2\sigma(F)$). Discrete anions that contain octahedral "TeO_6" and "PdO_6" units linked via edge sharing are present in the solid. The structure of the platinum complex $K_6Na_2[Pt(OH)_2(HTeO_6)_2]\cdot 12H_2O$ has been determined. Crystals were found to be monoclinic, space group $C2/m$, with $a = 21.099$ (11) Å, $b = 6.778$ (3) Å, $c = 9.041$ (4) Å, $\beta = 92.10$ (4)°, $V = 1292.1$ Å^3, and $Z = 2$. The structure was refined to $R = 0.041$ from 1170 data ($F > 3\sigma(F)$) and contains discrete anions. Each anion has two bidentate chelate $[HTeO_6]^{5-}$ units bonded to an octahedrally coordinated Pt atom. No H atoms were located. ^{125}Te and ^{195}Pt NMR and EXAFS data are used to identify other species present in solution.

Introduction

Tellurates ($H_{6-n}TeO_6^{n-}$) and periodates ($H_{5-n}IO_6^{n-}$) are known for their ability to stabilize transition-metal centers in high oxidation states. In addition to their inherent interest as examples of rare oxidation states, such materials are often strong multielectron oxidants and have considerable synthetic potential in this role.[2] The known complexes[2] range from extended lattices to discrete anions, and their correct formulation in the absence of structural data is far from easy. A number of predicted structures have subsequently been shown to be erroneous in the light of crystallographic studies. Several structures of periodato complexes have been determined in recent years including those of V(V),[3] Ru(VI),[4] Co(III),[5] Cu(III),[6] and Ag(III),[6] but by contrast we believe that the only discrete transition-metal tellurate anion to be characterized by X-ray diffraction is $Na_5[Cu(H_2TeO_6)_2]\cdot 10H_2O$.[7] We have recently reported a reinvestigation of the periodato complexes of palladium(IV) and platinum(IV)[1] including the crystal structure of $K_4Na_2[Pt(OH)_2(HIO_6)_2]\cdot 10H_2O$. The corresponding tellurate systems have previously been the subject of two brief and inconclusive studies,[8,9] but we are now able to present the results of a detailed structural and spectroscopic investigation of these materials.

Experimental Section

Multinuclear NMR spectra were obtained on a Bruker AM360 spectrometer from aqueous solutions containing a small quantity of D_2O to provide the lock signal and with 10-mm o.d. tubes. Tellurium-125 (113.6 MHz) and platinum-195 (77.6 MHz) were referenced to neat Me_2Te and aqueous K_2PtCl_6, respectively. Raman spectra and analytical (EDX and TGA) data were obtained as described previously.[1] The EXAFS data were obtained at the Synchrotron Radiation Source, Daresbury, England, operating at 2 GeV with an average ring current of 130 mA. Pd K-edge data were recorded on station 9.2 using a double-crystal silicon(220) monochromator, and Pt L_{III}-edge data, on station 7.1 using an order-sorting silicon(111) monochromator. Data were collected in transmission mode from 4 mm path length glass solution cells with Mylar windows. Data analysis utilized standard procedures that have been previously described.[1]

Preparation of $Na_{12}H_2[Pd_2Te_4O_{24}H_2]\cdot 20H_2O$. $PdCl_2$ (0.2 g, 1.13 mmol) was dissolved in H_2O (20 mL) containing a few drops of concentrated HCl. Chlorine gas was bubbled through this solution until no further color change occurred followed by nitrogen to purge the solution of excess chlorine. Telluric acid (0.53 g, 2.3 mmol) and NaOH (to ca.

(1) Part 36: Levason, W.; Spicer, M. D.; Webster, M. *J. Coord. Chem.*, in press.
(2) Downs, A. J.; Adams, C. J. In *Comprehensive Inorganic Chemistry*; Bailar, J. C., Emeleus, H. J., Nyholm, R. S.; Trotman-Dickenson, A. F., Eds.; Pergamon: Oxford, England, 1982; Vol. 2, pp 1452-1456.
(3) Michiue, Y.; Ichida, H.; Sasaki, Y. *Acta Crystallogr., Sect. C* **1982**, *C43*, 175.
(4) El-Hendawy, A. M.; Griffith, W. P.; Piggott, B.; Williams, D. J. *J. Chem. Soc., Dalton Trans.* **1988**, 1983.
(5) Lebioda, L.; Ciechanowicz-Rutkowska, M.; Baker, L. C. W.; Growchowski, J. *Acta Crystallogr., Sect. B* **1980**, *B36*, 2530.
(6) Adelskold, V.; Eriksson, L.; Wang, P.-L.; Werner, P.-E. *Acta Crystallogr., Sect. C* **1988**, *C44*, 597. Masse, R.; Simon, A. *J. Solid State Chem.* **1982**, *44*, 201.
(7) Levason, W.; Spicer, M. D.; Webster, M. *J. Chem. Soc., Dalton Trans.* **1988**, 1377.
(8) Siebert, H.; Mader, W. *Z. Anorg. Allg. Chem.* **1967**, *351*, 146.
(9) Lister, M. W.; McLeod, P. *Can. J. Chem.* **1965**, *43*, 1720.

0020-1669/91/1330-0967$02.50/0